microbial biotechnology

Open Access

Design and engineering of whole-cell biocatalyst for efficient synthesis of (*R*)-citronellal

Baoqi Zhang, Han Du, Yanqiu Zheng, Jiale Sun, Yu Shen, Jinping Lin* and Dongzhi Wei

State Key Laboratory of Bioreactor Engineering, New World Institute of Biotechnology, East China University of Science and Technology, Shanghai, 200237, China.

Summary

Bioproduction of optical pure (*R*)-citronellal from (*E*/*Z*)-citral at high substrate loading remains challenging. Low catalytic efficiency of (*R*)-stereoselective ene reductases towards crude citral mixture is one of the major bottlenecks. Herein, a structure-based engineering strategy was adopted to enhance the catalytic efficiency and stereoselectivity of an ene reductase (OYE2p) from *Saccharomyces cerevisiae* YJM1341 towards (*E*/*Z*)-citral. On basis of homologous modelling, molecular docking analysis and alanine scanning at the binding pocket of OYE2p, a mutant Y84A was obtained with simultaneous increase in catalytic efficiency and stereoselectivity. Furthermore, site-saturation mutagenesis of Y84 yielded seven mutants with improved activity and stereoselectivity in the (*E*/*Z*)-citral reduction. Among them, the variant Y84V exhibited an 18.3% and 71.3% rise in catalytic efficiency (k_{cat}/K_m) for (*Z*)-citral and (*E*)-citral respectively. Meanwhile, the stereoselectivity of Y84V was improved from 89.2% to 98.0% in the reduction in (*E*/*Z*)-citral. The docking analysis and molecular dynamics simulation of OYE2p and its variants revealed that the substitution Y84V enabled (*E*)-citral and (*Z*)-citral to bind with a smaller distance to the key hydrogen donors at a modified (*R*)-selective binding mode. The variant Y84V was then co-expressed with glucose dehydrogenase from *Bacillus megaterium* in *E. coli* D4, in which competing *prim*-alcohol dehydrogenase genes were deleted to prevent the undesired reduction in the aldehyde moiety of citral and citronellal. Employing this biocatalyst, 106 g l^{-1} (*E*/*Z*)-citral was completely converted into (*R*)-citronellal with 95.4% *ee* value and a high space-time yield of 121.6 g l^{-1} day^{-1}. The work highlights the synthetic potential of Y84V, which enabled the highest productivity of (*R*)-citronellal from (*E*/*Z*)-citral in high enantiopurity so far.

Introduction

(*R*)-citronellal is a valuable intermediate for the industrial production of (-)-menthol, one of the most crucial flavouring compounds with an annual worldwide demand of more than 30000 tons (Lenardão *et al*., 2007; Salminen and Virtanen, 2014; Zuliani *et al*., 2020). At present, transition metal-catalysed stereoselective reduction in citral (a mixture of trans- and cis-isomer) was the main synthetic method for (*R*)-citronellal, which was used as a chiral precursor for the industrial synthesis of (-)-menthol in the Takasago and BASF process (Etzold and Jess, 2009; Zuliani *et al*., 2020). In the asymmetric organocatalysis, the prior separation of (*E*)-citral and (*Z*)-citral by a chemical or physical process is necessary since the optical purity of (*R*)-citronellal yield by (*E*)-citral is higher than (*Z*)-citral. Furthermore, these metal catalysts have some shortcomings such as difficult to reuse, low chemical selectivity and high reaction temperature requirement (Maeda *et al*., 2012). Therefore, the biosynthesis of (*R*)-citronellal from (*E*/*Z*)-citral is attracting considerable attention for overcoming citral isomer separation.

Previously, several ene reductases from the old yellow enzyme (OYE) family have been identified to synthesize (*R*)-citronellal, but most of them showed low activity and insufficient stereoselectivity (Toogood and Scrutton, 2019). So far, only a few examples of ene reductases have been reported to be able to produce (*R*)-citronellal from (*E*/*Z*)-citral. As a representative example, the NADPH-dependent ene reductase OYE2.6 from *Saccharomyces cerevisiae* was employed in preparing (*R*)-citronellal from 50 mM (*E*/*Z*)-citral (an approximately 3:2 mixture of both isomers) with 90.0% *ee* (Bougioukou and Walton, 2010). Protein engineering of ene reductase has

Received 8 July, 2021; accepted 12 October, 2021.
*For correspondence. E-mail jplin@ecust.edu.cn; Tel. +86 21 64251923; Fax +86 21 64250068.
Microbial Biotechnology (2022) **15**(5), 1486–1498
doi:10.1111/1751-7915.13958
Funding Information
This work was supported by the National Key Research and Development Program of China (No. 2021YFC2102100), the Natural Science Foundation of Shanghai (No. 19ZR1412700), the Fundamental Research Funds for the Central Universities (No. 22221818014) and partially supported by the Open Funding Project of the State Key Laboratory of Bioreactor Engineering.

been focused on changing its stereoselectivity or catalytic activity (Amato and Stewart, 2015; Toogood and Scrutton, 2019; Liu *et al*., 2021a, 2021b). The variant W66A/I231A of NCR from *Zymomonas mobilis* obtained by Hauer and co-workers reversed the exclusively (*S*)-selective towards (*E*)-citral from 99% (*S*) to 63% (*R*), and the (*Z*)-citral derived stereoselectivity was decreased from 99% (*S*) to 81% (*S*) respectively (Kress and Rapp, 2017). The variant P76 M/R330H of OYE2y from *S. cerevisiae* CICC1060 and the variant C25G of XenA from *Pseudomonas putida* were reported to yield optically pure (*R*)-citronellal (> 99% ee), whereas lower product yields (15.8–33.5%) were achieved at merely 5–20 mM (*E*/*Z*)-citral (Yanto *et al*., 2010; Ying *et al*., 2019). Apparently, the low catalytic activity and undesirable stereoselectivity of reported ene reductases could not meet the industrial application in biosynthesis of (*R*)-citronellal.

Due to the time-consuming and costly purification of enzymes, and the complexity of cofactor recycling, the vast majority of red-ox biotransformations have been performed using whole-cell catalysts (Hepworth *et al*., 2017). Although bioreduction of (*E*/*Z*)-citral to (*R*)-citronellal using whole-cell biocatalyst is an attractive route (Fig. 1), undesired formation of nerol/geraniol and citronellol via the reduction in the aldehyde moiety due to the presence of competing aldo-keto reductases (AKRs) and alcohol dehydrogenases (ADHs) in the whole cells, leading to the poor chemoselectivity of whole-cell bioreduction of citral (Bougioukou *et al*., 2010; Kunjapur and Tarasova, 2014). Zhou *et al*. (2014) reported that three endogenous enzymes (YjgB, AdhP and YahK) in *E. coli* MG1655 could catalyse the reduction in geranial into geraniol. Therefore, characterization and deletion of the interfering ADHs and AKRs are essential for developing the whole-cell catalysts for efficient biosynthesis of (*R*)-citronellal.

Previously, we identified an NADH-dependent ene reductase OYE2p (Accession Number: AJV32222.1) from *S. cerevisiae* YJM1341, which exhibited an excellent *ee* of 98.9% (*R*) towards (*E*)-citral and a moderate *ee* of 88.8% (*R*) towards (*E*/*Z*)-citral at a substrate loading of 200 mM (Zheng *et al*., 2018). Herein, we attempted to engineer OYE2p for improving stereoselectivity and activity towards (*E*/*Z*)-citral. By screening of the key residues at the substrate-binding pocket, an excellent variant Y84V with remarkably enhanced activity and *R*-stereoselectivity was obtained. Besides, the key endogenous enzymes in *E. coli* BL21(DE3) that might catalyse the reduction in the aldehydes were deleted through gene editing to impair the undesired reduction in the aldehyde moiety in both substrate and product. Then, variants Y84V and *Bm*GDH were co-expressed in the engineered *E. coli*. By using the whole cells of the engineering *E. coli* as the biocatalyst, a systematic optimization of the reaction conditions enabled production of (*R*)-citronellal from (*E*/*Z*)-citral on a hundred gram scale.

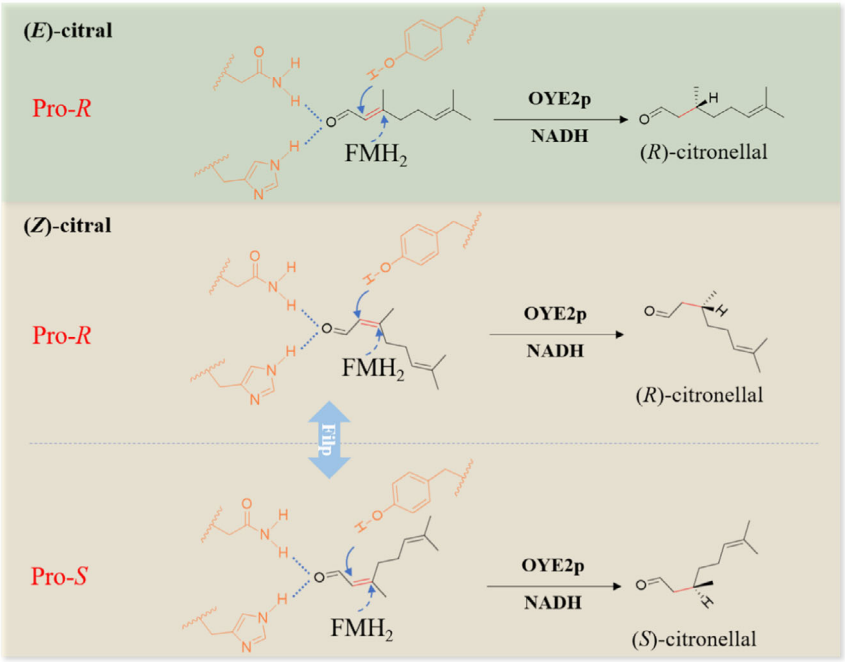

Fig. 1. OYE2p-mediated reduction in (*E*/*Z*)-citral to (*R*)- and (*S*)-citronellal.

Results and discussion

Structure-based engineering of OYE2p

The amino acid residues lining the substrate-binding pocket were more likely to have a profound effect on the enzyme activity and stereoselectivity. A structure-guided engineering strategy focusing on the active site amino acids was applied for creating highly active variants. The structure mode of OYE2p was built using the modeller 9.20 program based on the known structure of OYE1 (PDB ID: 3TX9) from *S. pastorianus* and OYE3 (PDB ID: 5V4P) from *S. cerevisiae*. The template protein showed 91.3% (OYE1) and 80.8% (OYE3) sequence identity with OYE2p. Model evaluation was performed using the Verify-3D and Ramachandran plot web server (Lüthy and Bowie, 1992; Hooft and Sander, 1997). The Verify-3D analysis results pointed out that the amino acid 3D-1D score was above 0.2 (Fig. S1A). Ramachandran plot analysis results showed that 100% of the residues fell into the favoured and allowed region (Fig. S1B). Overall, the evaluation results indicated that our model of OYE2p was reliable.

To probe the key amino acid residues that might affect catalytic activity and stereoselectivity, molecular docking analysis was performed on OYE2p using the Autodock 4.2 program. Similar to all ene reductases, the conserved catalytic pattern HxxH/NxY was generally found at the catalytic centre of OYE2p (Fig. S2). Thus, (*E*)-citral and (*Z*)-citral were docked into the catalytic centre consisting of the catalytic triad (H193, N196 and Y198) respectively. OYE2p structures in complex with (*E*)-citral or (*Z*)-citral with the lowest binding energy were chosen, and all amino acids within 5 Å vicinity of the docked ligand were selected as the hot spots (Fig. 2). Among these 14 residues (Thr39, Met41, Tyr84, Trp118, Ala123, His193, Asn196, Tyr198, Arg245, Phe252, Asn253, Pro297, Phe298 and Tyr377), Tyr198 was the catalytic residue of OYE2p, and the 123 site was alanine. Therefore, these two amino acid residues were excluded from further alanine scanning.

Twelve key residues (Thr39, Met41, Tyr84, Trp118, His193, Asn196, Arg245, Phe252, Asn253, Pro297, Phe298 and Tyr377) were subjected to alanine scanning mutagenesis, and the activities and stereoselectivities

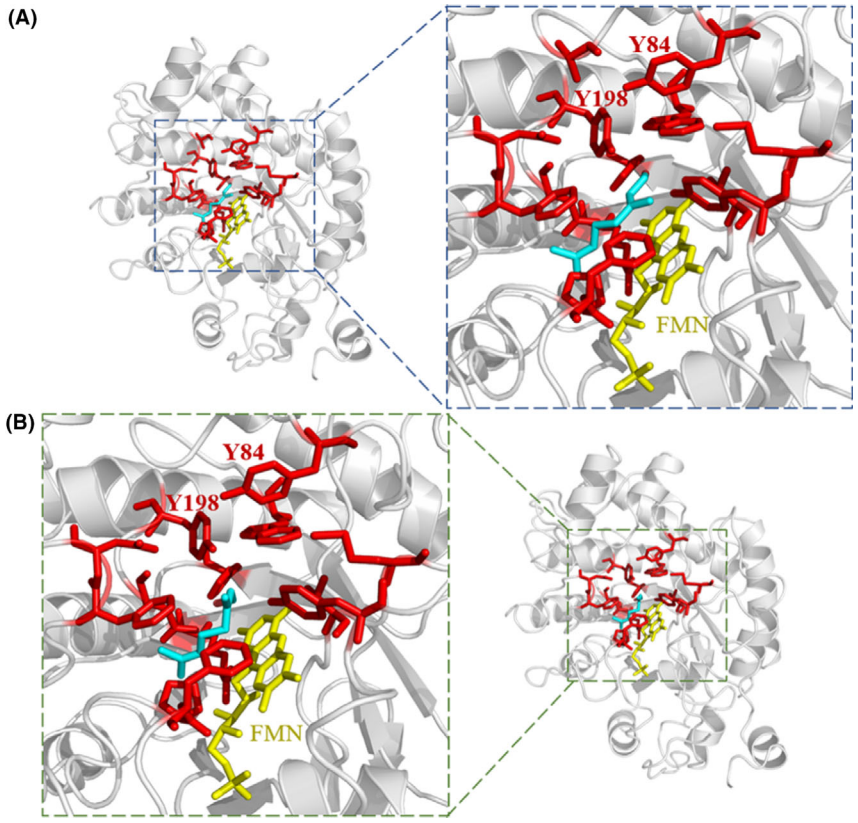

Fig. 2. Structure analysis of wild type OYE2p.
A. molecular docking analysis of (*E*)-citral into the catalytic centre of OYE2p, (B) molecular docking analysis of (*Z*)-citral into the catalytic centre of OYE2p. Residues (in red) within the substrate-binding pocket of OYE2p within a 5 Å vicinity of the docked ligand.

towards (*E*/*Z*)-citral were determined. SDS-PAGE analysis showed that all mutants were successfully expressed in *E. coli* BL21(DE3) in a soluble form at almost the same expression level (Fig. S3). As shown in Table 1, compared with wild type OYE2p, variants Y84A, P297A and F298A showed higher activities, while other variants exhibited significantly decreased activity and stereoselectivity. Among the three variants with improved activities, (*R*)-selectivities of P297A and F298A were significantly diminished, suggesting that both single-site changes were a trade-off between activity and stereoselectivity. By contrast, substituting Ala for Tyr84 remarkably increased activity for (*E*/*Z*)-citral with an increased enantiomeric excess from 89.2% (*R*) to 94.0% (*R*). Thus, site-directed saturation mutagenesis was subsequently performed to assess the effects of alteration of the Tyr84 site.

Table 1. Alanine scanning of 12 key residues of OYE2p towards (*E*/*Z*)-citral reduction.

Enzyme	Relative activity (%)	*ee* of (*R*)-citronellal (%)
WT	100 ± 3.9	89.2
T39A	0	–
M41A	55.8 ± 2.6	70.8
Y84A	125.3 ± 7.6	94.0
W118A	0	–
H193A	0	–
N196A	5.9 ± 1.1	76.1
R245A	0	–
F252A	44.2 ± 6.4	21.4
N253A	48.0 ± 2.9	80.7
P297A	116.8 ± 8.2	46.6
F298A	119.7 ± 4.7	48.7
Y377A	11.9 ± 3.8	81.2

Reaction conditions: 100 mM PBS (pH 8.0), 50 mM (*E*/*Z*)-citral, 75 mM glucose, 0.2 mM NAD^+, 20 g l^{-1} OYE2p (WT or variants) and 5 g l^{-1} *Bm*GDH using lyophilized *E. coli* cells.

All variants at Y84 residue were expressed in a soluble form in *E. coli* BL21(DE3) with similar molecular weights to wild type OYE2p at almost the same expression level (Fig. S4). As presented in Fig. 3, compared with WT, eight variants exhibited enhanced activities, including Y84A, Y84V, Y84L, Y84I, Y84S, Y84T, Y84C and Y84D. Meanwhile, nine variants showed the improved stereoselectivities, including Y84A, Y84P, Y84V, Y84L, Y84I, Y84M, Y84F, Y84T and Y84R. Among them, only five variants, Y84A, Y84V, Y84L, Y84I and Y84T, showed simultaneous improvement in stereoselectivity and activity. Noticeably, the variant Y84V showed the highest activity and the highest stereoselectivity of 98.0%. From these variants with improved stereoselectivity, according to the side-chain volume of amino acids, a steric trend was observed in the reduction in citral under different hydrophobic amino acid substitution at 84 site. Except for glycine substitution, changing Tyr84 to smaller hydrophobic residues somewhat promoted the (*R*)-stereoselectivity towards (*E*/*Z*)-citral.

Furthermore, variant Y84V was used in the reduction in both isomers of (*E*/*Z*)-citral. It was noted that the effects on catalytic activity and stereoselectivity for both isomers were different (Table 2). Replacing Tyr84 with Val increased the stereoselectivity towards (*Z*)-citral (from 68.3% *ee* (*R*) to 90.1% *ee* (*R*)), while keeping high stereoselectivity towards (*E*)-citral (99.4% *ee* (*R*)). Meanwhile, Y84V mutant exhibited increased specific activities towards two isomers (0.232 U mg^{-1} for (*E*)-citral and 0.069 U mg^{-1} for (*Z*)-citral), which was consistent with the improved activity towards (*E*/*Z*)-citral. These results implied that the stereoselectivity and catalytic activity of OYE2p can be improved through Val substitution in the 84 site.

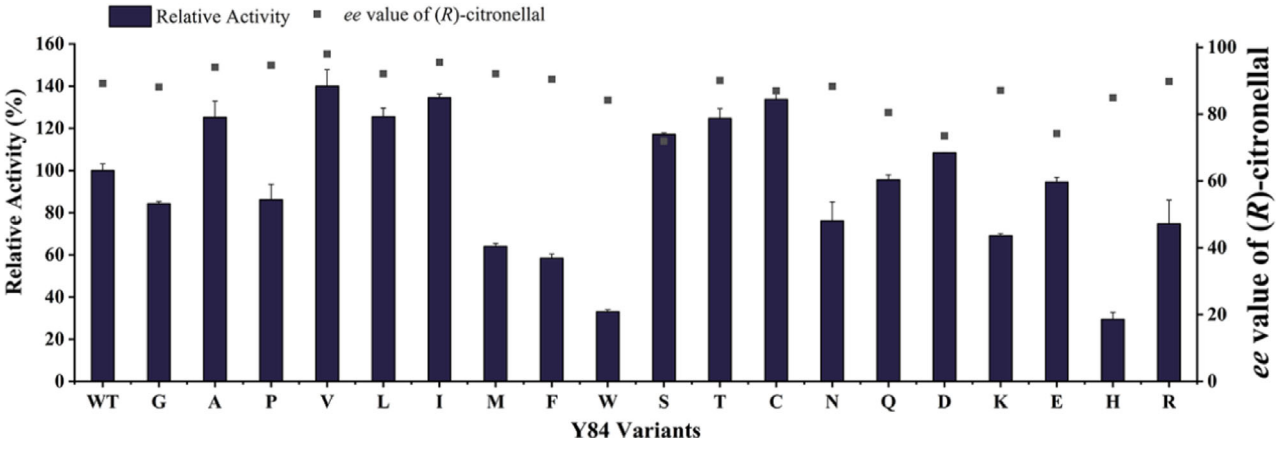

Fig. 3. Relative activity and stereoselectivity of OYE2p Y84 site variants towards (*E*/*Z*)-citral. Reaction conditions 100 mM PBS (pH 8.0), 50 mM (*E*/*Z*)-citral, 75 mM glucose, 0.2 mM NAD^+, 20 g l^{-1} OYE2p (WT or variants) and 5 g l^{-1} *Bm*GDH using lyophilized *E. coli* cells.

Table 2. Specific activities and stereoselectivities of WT and Y84V toward (*E*)-citral and (*Z*)-citral.

	(*E*)-citral		(*Z*)-Citral	
Enzyme	Specific activity[a] (U mg^{-1})	*ee* of (*R*)-citronellal[b] (%)	Specific activity[a] (U mg^{-1})	*ee* of (*R*)-citronellal[b] (%)
WT	0.174 ± 0.022	98.9	0.040 ± 0.010	68.3
Y84V	0.232 ± 0.046	99.4	0.069 ± 0.013	90.1

a. Specific activity was determined with purified proteins. Reaction conditions: 100 mM PBS (pH 8.0), 10 μg purified protein, 0.2 mM NADH, 5 mM substrate and at 30°C.
b. *ee* value was analysed by GC. Reaction conditions were the same as described in the Table 1.

For an accurate assessment of catalytic efficiency and to elucidate the origin of the increased reduction activity, the kinetic parameters of WT and Y84V were investigated. Compared with the wild type OYE2p, the variant Y84V showed a 71.3% increase in catalytic efficiency (k_{cat}/K_m) towards (*E*)-citral (Table 3). Correspondingly, the enhancement in k_{cat}/K_m was attributed to the increase in k_{cat} and the decrease in the K_m. For (*Z*)-citral, Y84V displayed an 18.3% increase in k_{cat}/K_m, which mainly benefited from the increased k_{cat}. The results also revealed that both WT and Y84V displayed a preference for (*E*)-citral over (*Z*)-citral. Moreover, for the cofactor NADH, K_m value of Y84V was increased in comparison with wild type, which suggested that variant Y84V had a decreased affinity for NADH.

To gain structural insights into the superior performance of Y84V, molecular docking simulation was performed with Y84V and WT using (*E*)-citral and (*Z*)-citral as the ligand respectively (Fig. 4A, D and Fig. S5A, D). According to the catalytic mechanism of ene reductase, the Tyr198 and $FMNH_2$ donated their hydrogen atoms to the C=C bond of citral, thereby activating the reaction. Hence, the distance (D1) from Tyr198-OH to substrate α-C and the distance (D2) from FMN-N5 to substrate β-C could show how difficult it is to react. Molecular dynamic (MD) simulations for WT and Y84V with both isomers were carried out as well. As shown in Fig. 4B and E, both D1 and D2 for (*E*)-citral in Y84V were significantly shorter than that of the WT, which was beneficial for the nucleophilic attack on the C=C bond of (*E*)-citral. The same performance was observed in MD simulations for WT and Y84V with (*Z*)-citral (Fig. S5). Correspondingly, compared with WT, the catalytic efficiency of Y84V towards (*E*)-citral and (*Z*)-citral was increased by approximately 71% and 18% respectively (Table 3). When Tyr84 was mutated into valine, the space in the binding pocket was expanded from 357 Å^3 to 377 Å^3 (Fig. S6). Furthermore, the tilted binding position of (*Z*)-citral was observed in Y84V-(*Z*)-citral complex (Fig. 5A and B), whereas there was a change in the angle (θ1) between the vector *v*1 (α-C and β-C of (*Z*)-citral) and *v*2 (normal vector of FMN plane) (Fig. 5C). The relative position between the conjugate plane of substrate and FMN plane was described by the angle between *v*1 and *v*2. In the WT-(*Z*)-citral complex, there is a kink in the α-C and β-C of (*Z*)-citral (average values of θ1=97.7°), and the kink is less prominent in Y84V-(*Z*)-citral complex (average values of θ1=94.7°), which produced a modified (*R*)-selective binding mode for (*Z*)-citral (Fig. 5D). These results indicated that the Y84V mutant allowed the substrates to enter into the active centre pocket at an (*R*)-selectivity binding mode and a closer distance with proton donors.

Table 3. Kinetic parameters of WT and Y84V toward (*E*)-citral and (*Z*)-citral.

		Enzyme	
Value for:	Parameter	WT	Y84V
(*E*)-citral[a]	K_m (mM)	0.120 ± 0.025	0.107 ± 0.026
	k_{cat} (S^{-1})	0.213 ± 0.008	0.326 ± 0.016
	k_{cat}/K_m (S^{-1}*mM^{-1})	1.777 ± 0.305	3.045 ± 0.594
(*Z*)-citral[a]	K_m (mM)	0.310 ± 0.047	0.326 ± 0.084
	k_{cat} (S^{-1})	0.130 ± 0.008	0.162 ± 0.008
	k_{cat}/K_m (S^{-1}*mM^{-1})	0.421 ± 0.039	0.498 ± 0.104
NADH[b]	K_m (mM)	0.014 ± 0.004	0.027 ± 0.008

a. Reaction conditions: 100 mM PBS (pH 8.0), 10 μg purified protein, 0.2 mM NADH, substrate (0.01–10 mM) and at 30°C.
b. Reaction conditions: 100 mM PBS (pH 8.0), 10 μg purified protein, 5 mM (*E*/*Z*)-citral, NADH (0.005–0.5 mM) and at 30°C.

Optimization of E. coli *BL21(DE3) by deleting endogenous enzymes enable by-products formation*

To develop a more attractive synthesis process of (*R*)-citronellal, the use of purified ene reductases has been explored but requiring additional production costs (Bougioukou *et al*., 2010). By contrast, whole-cell biocatalyst had many advantages over using pure proteins, which makes it ideal for the production of (*R*)-citronellal. It is notable that *E. coli* has many endogenous AKRs and ADHs that could convert aldehydes to alcohols (Kunjapur *et al*., 2014). For instance, three native enzymes (YjgB, AdhP and YahK) in *E. coli* MG1655 could

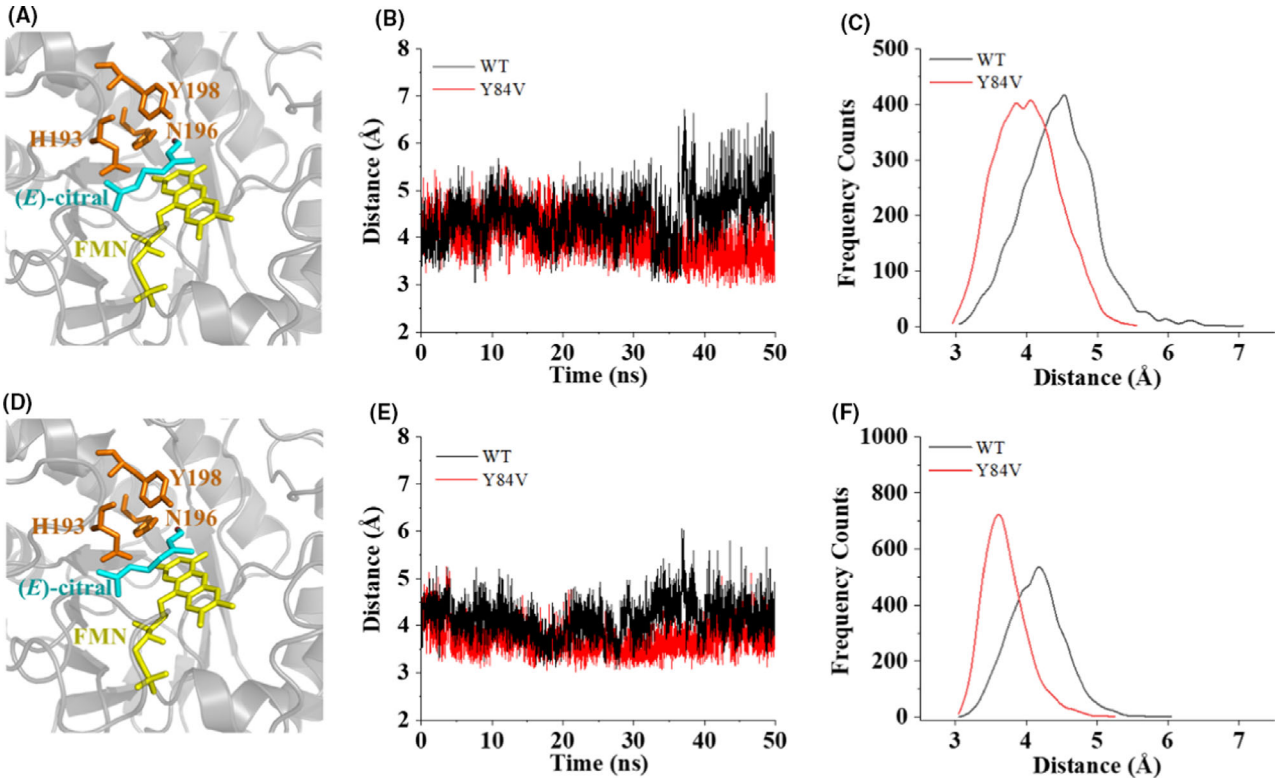

Fig. 4. Docking and molecular dynamic simulation analysis of WT and Y84V.
A. Molecular docking of (*E*)-citral into the active sites of wild type OYE2p.
B. Distance between hydroxyl group of Tyr198 and α-C of (*E*)-citral in Y84V-(*E*)-citral complex (red) and WT-(*E*)-citral complex (black).
C. Distribution of the distance between hydroxyl group of Tyr198 and α-C of (*E*)-citral in Y84V-(*E*)-citral complex (red) and WT-(*E*)-citral complex (black).
D. Molecular docking of (*E*)-citral into the active sites of Y84V.
E. Distance between N5 atom of FMN and β-C of (*E*)-citral in Y84V-(*E*)-citral complex (red) and WT-(*E*)-citral complex (black).
F. Distribution of the distance between N5 atom of FMN and β-C of (*E*)-citral in Y84V-(*E*)-citral complex (red) and WT-(*E*)-citral complex (black).

catalyse the reduction in geranial into geraniol (Zhou *et al*., 2014). AdhP (Accession Number: QJZ12150.1) and YahK (Accession Number: QJZ11098.1) also exist in *E. coli* BL21(DE3). To further determine the activity of endogenous enzymes towards (*E*/*Z*)-citral or citronellal, Selenzyme was applied into searching for the similarity between the target reaction and the catalytic reaction carried out by AKRs and ADHs in *E. coli* BL21(DE3) (Table S3) (Carbonell *et al*., 2018). The results suggested that alcohol dehydrogenases AdhP and AdhE (Accession Number: QJZ11959.1) could catalyse the reduction in (*E*/*Z*)-citral and citronellal.

For further probing the contribution of these alcohol dehydrogenases in alcohol by-products formation, AdhP, AdhE and YahK genes were cloned into the pET-28a(+) vector and overexpressed in *E. coli* BL21 (DE3), individually. After Ni-NTA purification procedure (Fig. S8), the purified enzymes were used to assess the catalytic activity against (*E*)-citral, (*Z*)-citral and citronellal respectively. As expected, these enzymes have catalytic activity for the tested substrates. In particular, AdhP had a much higher catalytic activity towards (*E*)-citral (15.7 U mg^{-1}) (Fig. 6A). In addition, AdhP displayed a higher activity towards citronellal (12.0 U mg^{-1}), approximately twice higher than that of AdhE and YahK. For (*Z*)-citral, YahK showed a marked higher activity of 20.1 U mg^{-1} (3.88-fold higher than AdhP).

Next, a four-gene deleted *E. coli* BL21(DE3) which was named *E. coli* D4 was constructed by deleting the genes *yahK*, *adhP, adhE* and *nemA* (Accession Number: QJZ11098.1) encoding an ene reductase, which catalyse citral to (*S*)-citronellal (Mueller *et al*., 2010) (Table S5, Fig. S9). *In E. coli* D4, *Bm*GDH (Accession Number: 3AUS_A) for the regeneration of NADH *in situ* was expressed, and the obtained strain *E. coli* D4/GDH was employed in catalysing citral and citronellal to further evaluate the effect of these enzymes on by-product formation. As shown in Fig. 6B, deletion of *yahK*, *adhP, adhE* and *nemA* had effects on by-products (citronellol, geraniol and nerol) formation. The control strain *E. coli* BL21(DE3)/GDH converted 44.8% of the citronellal into citronellol in presence of glucose, while conversion of

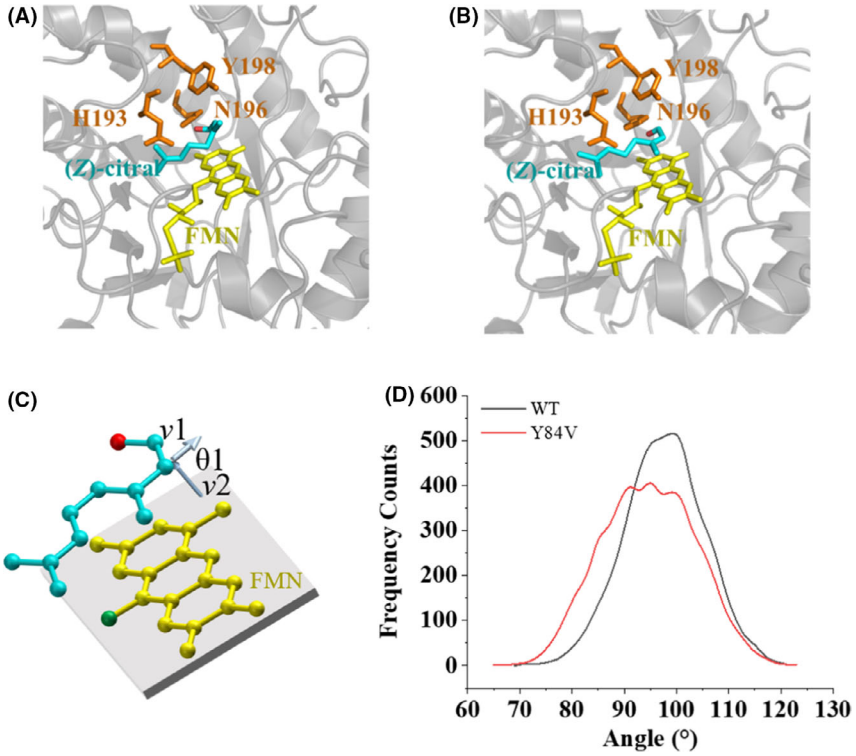

Fig. 5. Molecular docking of (*Z*)-citral into the active sites of WT (A) and Y84V (B).
C. Vectors defined to compute the motions of the (*Z*)-citral. The change in binding mode was given by θ1, the angle between vector *v*1 (α-C and β-C of (*Z*)-citral) and *v*2 (normal vector of FMN surface).
D. Distribution of the angle θ1 in Y84V-(*Z*)-citral complex (red) and WT-(*Z*)-citral complex (black).

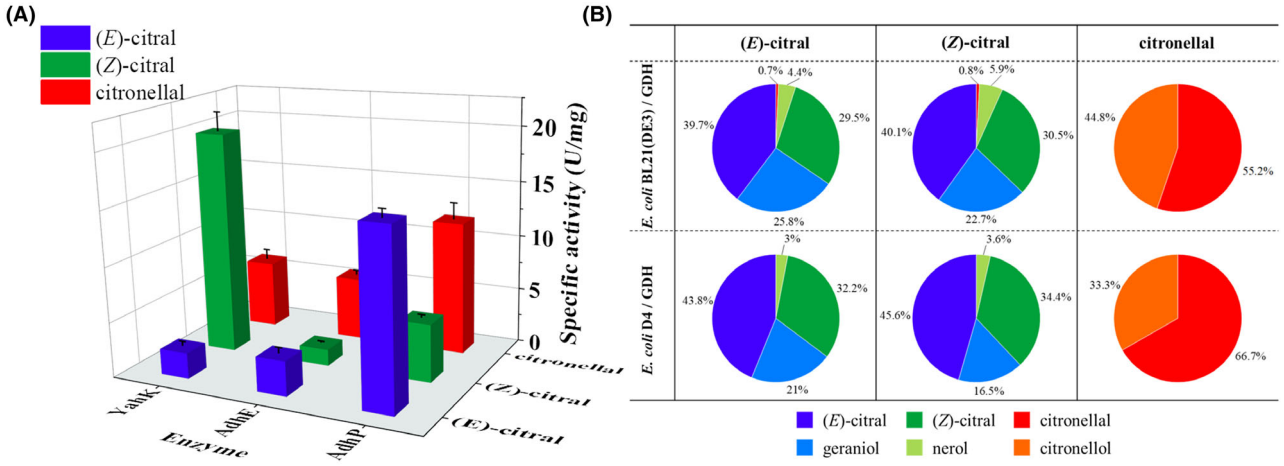

Fig. 6. A. Specific activity of AdhP, YahK and adhE towards (*E*)-citral, (*Z*)-citral and citronellal.
B. Reduction in (*E*)-citral, (*Z*)-citral and citronellal using *E. coli* BL21(DE3)/GDH and *E. coli* D4/GDH. The changes in geranoids from reaction mixture are shown with a pie chart.

citronellal to citronellol was significantly dropped to 33.3% by *E. coli* D4/GDH. Similar patterns were observed when feeding (*E*)-citral or (*Z*)-citral, the yield of by-products was reduced by 22.1% and 32.0% respectively.

Using the engineered strain *E. coli* D4 as the host, the best variants Y84V and *Bm*GDH were co-expressed and the whole cells of the obtained strain *E. coli* D4/Y84V/GDH (D4-VG) were employed for the asymmetric reduction in (*E*/*Z*)-citral. The recombinant *E. coli* BL21(DE3)/

Y84V/GDH (BL21-VG) using *E. coli* BL21(DE3) was as a control. SDS-PAGE analysis showed that Y84V and *Bm*GDH were successfully expressed in *E. coli* BL21 (DE3) and *E. coli* D4 at almost the same expression level (Fig. S10). Results showed that deletion of these aldehyde reductase genes was beneficial for the citronellal production (Fig. S11). Overall, these results suggested the feasibility of impairing the aldehyde reduction in substrate and product during citronellal bioproduction.

*Selection of the optimal reaction condition for an efficient production of (*R*)-citronellal by* E. coli *D4/Y84V/GDH*

In order to improve the catalytic efficiency of whole cells of *E. coli* D4/Y84V/GDH, the reaction conditions including pH value, temperature and NAD^+ concentration were investigated and optimized. The effect of pH on the asymmetric reduction in citral to (*R*)-citronellal was performed using lyophilized cells in aqueous buffers with different pH values. As shown in Fig. 7A, the optimum pH was determined to be 8.0, which was close to the optimal pH of Y84V (7.5) and *Bm*GDH (around 8.0) respectively (Baik *et al*., 2003; Zheng *et al*., 2018). Moreover, citronellal production dropped rapidly when the pH values higher than 8.5 or lower than 7.0, probably due to the reduced stability and activity of Y84V. Furthermore, the impact of pH value on *ee* value was remarkable. Yield and *ee* value of (*R*)-citronellal had no significant decrease when pH values between 7.5 and 8.5. Nevertheless, the *ee* value of (*R*)-citronellal was diminished to 95.3% when pH was changed to 6.0 (in sodium phosphate buffer). These results demonstrate that the optimum pH value of this reaction was 8.0, at which the high yield and excellent stereoselectivity (> 98%) could be achieved.

The influence of the reaction temperature was investigated at pH 8.0 and various temperatures, ranging from 20 to 37°C. According to the temperature-yield histogram (Fig. 7B), the product concentration of (*R*)-citronellal was increased from 52.8 ± 3.1 to 81.1 ± 3.5 mM with the rise of temperature from 20 to 30°C. Besides, further growth of the reaction temperature could not further increase the product concentration, which was owing to the deactivation of Y84V. These results revealed that the optimal reaction temperature was determined to be 30°C. The effects of NAD^+ concentration on citral reduction were investigated at pH 8.0 and 30°C under various NAD^+ concentrations of 0, 0.1, 0.2, 0.3 and 0.5 mM. As shown in Fig. 7C, the maximum yield of citronellal was obtained at 0.1 mM NAD^+ which exhibiting 5.32% improvements in citronellal production compared with no addition of NAD^+. The result indicates that the coenzyme of the recombinant cell can basically meet the needs of the reaction and avoid the requirement for additional cofactors in the bioproduction of (*R*)-citronellal.

The high stereoselectivity of Y84V towards citral makes it possible to perform well in the synthesis of (*R*)-citronellal. To effectively synthesize (*R*)-citronellal at the gram scale, asymmetric reduction of 106.6 g l^{-1} (*E*/*Z*)-citral by D4-VG (*E. coli* D4/Y84V/GDH) was performed

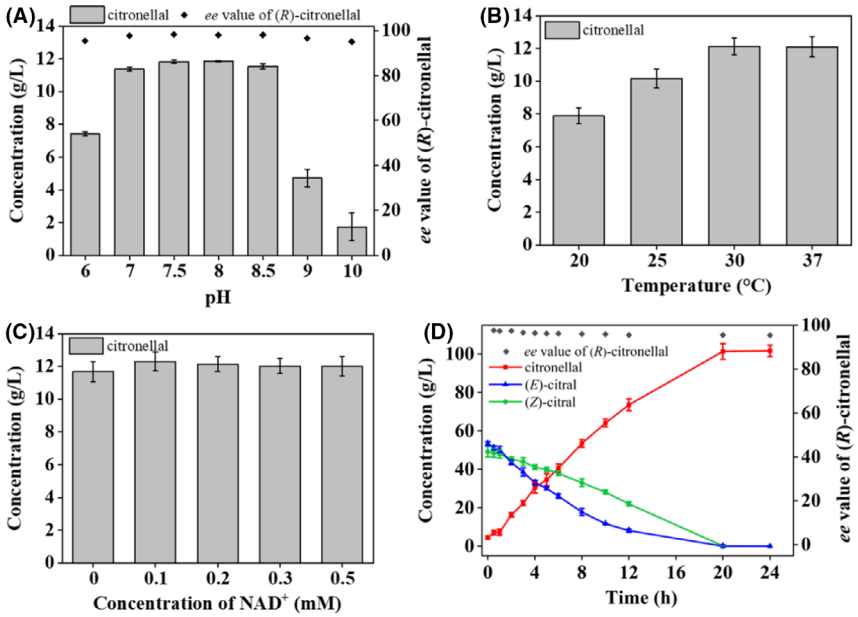

Fig. 7. Effect of pH (A), temperature (B) and NAD^+ concentration (C) on asymmetric (*R*)-citronellal synthesis by *E. coli* D4/Y84V/GDH (D4-VG). D. Synthesis of (*R*)-citronellal by D4-VG under optimized reaction conditions. Reaction conditions: 100 mM PBS (pH 8.0), 75 g l^{-1} D4-VG (lyophilized cells), 106.6 g l^{-1} (*E*/*Z*)-citral, 138.6 g l^{-1} glucose, 0.1 mM NAD^+ and at 30°C.

in 20 ml volume under optimized reaction conditions. The same reaction catalysed by the wild type OYE2p-expressing strain E. coli D4/OYE2p/GDH (D4-YG) was taken as control. As shown in Fig. 7D and Fig. S12, the D4-VG displayed pronounced catalytic efficiency towards (*E*/*Z*)-citral compared with (D4-YG). With 106.6 g l^{-1} (*E*/*Z*)-citral, the D4-VG achieved 100% conversion after 20 h, resulting in (*R*)-citronellal with 95.4% *ee* value and 121.6 g l^{-1} d^{-1} space-time yield. In contrast, low space-time yield of 62.6 g l^{-1} day^{-1} and low *ee* value 85.3% were obtained for the D4-YG. The time-course assays (Fig. 7D) showed that the reaction rate of (*E*)-citral by D4-VG was higher than (*Z*)-citral, leading to fast reduction in (*E*)-citral within 12 h. This might be ascribed to the preference of Y84V for (*E*)-isomer over (*Z*)-isomer, which has also been mentioned in the study of other ene reductases (Bougioukou *et al*., 2010; Ni *et al*., 2014). After extraction and evaporation, 1.37 g of (*R*)-citronellal was isolated with 64.3% yield. To date, there are few ene reductases were reported to asymmetrically catalyse the reduction in (*E*/*Z*)-citral to (*R*)-citronella, due to the deficiency of (*R*)-selective ene reductase towards (*E*/*Z*)-citral. By contrast, our work presented an efficient whole-cell catalyst for (*R*)-citronellal via asymmetric reduction in (*E*/*Z*)-citral with excellent stereoselectivity at high substrate loading, giving the highest product titter and productivity.

Conclusion

Here, we attempted to engineer OYE2p for both improved activity and enhanced stereoselectivity towards (*E*/*Z*)-citral. We identified the key residue Tyr84 which played a role in determining the stereoselectivity and activity of OYE2p. The mutants Y84V showed (*R*)-selectivity for (*E*/*Z*)-citral with 98.0% *ee* compared to 89.2% *ee* of the OYE2p. Meanwhile, the variant Y84V exhibited an 18.3–71.6% increase in catalytic efficiency (k_{cat}/K_m) for (*E*)-citral and (*Z*)-citral, respectively, compared with the wild type OYE2p. Additionally, we have constructed an engineered *E. coli* BL21(DE3) strain (*E. coli* D4) that can accumulate citronellal as main products. This result was achieved by the deletion of four genes in *E. coli* BL21(DE3) strain via CRISPR/Cas9 gene-editing technology. After co-expression with *Bm*GDH and Y84V in *E. coli* D4, a whole-cell biocatalyst was obtained which allows the reduction in (*E*/*Z*)-citral mixture to (*R*)-citronellal. Employing this biocatalyst, 106.6 g l^{-1} (*E*/*Z*)-citral could be completely converted within 24 h under the optimized reaction conditions, resulting in (*R*)-citronellal with 95.4% *ee* and 121.6 g l^{-1} day^{-1} space-time yield. This is the highest substrate concentration ever reported involving the biosynthesis of (*R*)-citronellal. In summary, a whole-cell biocatalyst was tailored for the preparative synthesis of (*R*)-citronellal, and opening the possibility of employing microbial catalyst in the C=C bond reduction in α,β-unsaturated aldehydes.

Experimental procedures

Chemicals and materials

Citral was obtained from Aladdin (Shanghai, China). (*R*)-citronellal and (*S*)-citronellal were obtained from Sigma (St Louis, MO, USA). (*E*)-citral and (*Z*)-citral were obtained from Zhejiang NHU Co., Ltd (Zhejiang, China). NAD^+ and NADH were obtained from Yeasen Biotechnology (Shanghai, China). PCR primers were synthesized by Personal Biotechnology (Shanghai, China), and DNA sequencing was performed by Tsingke Biological Technology (Beijing, China). Yeast extract and peptone were purchased from Oxoid (Hampshire, UK). Other chemicals involved were analytical grade and purchased from Titan Scientific (Shanghai, China).

The FastPfu DNA polymerase for PCR amplifications was purchased from Transgen (Beijing, China). The fast DNA restriction enzymes for cloning were purchased from Thermo Fisher Scientific (Shanghai, China), and a HiPure Plasmid Micro Kit for plasmid extracting was purchased from Magen (Guangzhou, China).

E. coli BL21 (DE3) cells (Transgen, Beijing) were used for overexpression of protein. The pET-21d(+), pET-28a (+) and pACYC184 were used for gene expression. The pCas and pTargetT were used for gene deletions in *E. coli* BL21(DE3). LB medium was used for *E. coli* cultivation. Ampicillin and chloromycetin were used at concentrations of 50 and 34 mg l^{-1} respectively.

Protein expression and purification

The recombinant *E. coli* strains were cultured in LB medium at 37°C and 200 rpm. When the OD_{600} of the culture reached 0.6, recombinant genes expression was induced with 0.2 mM IPTG at 20°C and 175 rpm for another 12 h. After completion of inducing, the cells were harvested by centrifugation at 8000 *g*, 4°C for 10 min, and washed twice with 0.9% NaCl solution.

1.0 g cell pellet was resuspended in 20 ml PBS (100 mM, pH 7.4) at a final concentration of 50 $g_{(wet\ cell)}$ l^{-1} and then disrupted by ultrasonication in an ice water bath. The supernatant was collected by centrifugation at 12 000 *g*, 4°C for 30 min. Subsequently, the supernatant was loaded on a HisTrap HP column pre-equilibrated with 20 mM imidazole in PBS (20 mM, pH 7.4). The target protein bound the HisTrap HP columns and was eluted with an increasing gradient from 25 to 500 mM of imidazole in PBS (20 mM, pH 7.4). The effluent containing the target protein was collected and dialyzed with

PBS (20 mM, pH 7.4) containing 200 mM NaCl and 5% (v/v) glycerinum for desalting. The purified protein was concentrated using Millipore (10 kDa). The protein concentration was estimated with Bradford Protein Assay Kit, and the purity of the target protein was analysed by SDS-PAGE.

Site-directed mutagenesis

Mutagenesis of OYE2p was performed through inverse PCR using the mutation primers and a Fast Mutagenesis System (Transgen, Beijing, China), and the pET21d-*oye2p* plasmid was used as template. Subsequently, the reaction mixture of site-directed mutagenesis was transformed into *E. coli* DH5α cells and spread on LB-kanamycin agar plates. Afterwards, the colonies were sequenced to verify the mutagenesis. Then, the recombinant plasmids were introduced into the host *E. coli* BL21 (DE3).

Homology modelling, docking and MD simulation

The structural model of OYE2p was built using the modeller 9.20 program (Martí-Renom *et al.*, 2000) which used the crystal structure of OYE1 (PDB ID: 3TX9, 91.3% sequence identity to OYE2p) and OYE3 (PDB ID: 5V4P, 80.8% sequence identity to OYE2p) as templates. This model was evaluated via Ramachandran plot and Verify-3D.

In order to understand the interactions between the OYE2p and (*E*/*Z*)-citral, (*E*)-citral and (*Z*)-citral were docked into the active centre pocket of OYE2p using AutoDock 4.2 program respectively (Morris *et al.*, 2009). Structural analysis was performed using the PyMOL-edu program.

MD Simulation was performed using Gromacs 2019.6 with the GROMOS96 force field. PRODRG as an automated server for topology generation was utilized to generate ligand-related files. The enzyme-ligand complexes were immersed in a dodecahedron box of spc216 explicit water. Then, sodium ions were added to neutralize the system and energy minimization was achieved by the steepest descent algorithm. After energy minimization, the NVT and NPT equilibrations were implemented at 300 K for 100 ns respectively. Following this, Production MD simulation was performed for 50 ns.

Enzyme assay, kinetic parameters and catalytic efficiency determination

The specific activities of AdhP, YahK, AdhE, OYE2p and its variants were evaluated using the spectrophotometric analysis of NADH consumption at 340 nm. For calculation of NADH concentration, the molar extinction coefficient of 6.22 mM^{-1} cm^{-1} at 340 nm was used. The standard assay mixture contained 100 mM PBS (pH 8.0), 5 mM substrate, 0.2 mM NADH and an appropriate amount of purified enzyme and was carried out at 30°C. One unit of enzyme activity (U) was defined as the amount of enzyme that catalyses the oxidation of 1.0 μmol NADH per minute. Kinetic parameters of purified OYE2p and its variants were assayed by measuring enzyme activities in the presence of various substrate concentrations (0.01^{-1}0 mM) with the concentration of NADH kept at 0.2 mM. The parameters K_m value for NADH were determined over a range of NADH concentrations (0.005–0.5 mM) with a fixed (*E*/*Z*)-citral concentration of 5 mM. The K_m and V_{max} values were obtained from a non-linear fit of the initial velocity data to the Michaelis–Menten equation (Eq. 1) using Origin 2020b software (OriginLab, Northampton, MA, USA).

$$V = V_{max} \times \frac{[S]}{(K_m + [S])}. \quad (1)$$

The parameter k_{cat} was calculated from V_{max} and the concentration of enzymes (OYE2p or its variants) according to the following equation:

$$k_{cat} = \frac{V_{max}}{E_{total}}, \quad (2)$$

where V is the reaction rate, V_{max} is the maximum reaction rate, K_m is the Michaelis constant, [S] is the concentration of substrate, and E_{total} is the concentration of enzymes (OYE2p or its variants) in the reaction.

The catalytic activity and stereoselectivity of OYE2p and its variants were performed in a 500 μl reaction system containing 50 mM substrate, 75 mM glucose, 0.2 mM NAD^+, OYE2p (WT or variants) (20 g l^{-1}) and *Bm*GDH (5 g l^{-1}) which were prepared as lyophilized cells and 100 mM PBS (pH 8.0). After incubation at 30°C and 200 rpm for 2 h, the reaction mixture was extracted twice with 500 μl ethyl acetate and then analysed by gas chromatography (GC).

To evaluate the knockdown effects on by-product formation of these dehydrogenases, 50 mM substrate ((*E*)-citral or (*Z*)-citral or citronellal), 75 mM glucose, 0.2 mM NAD^+, lyophilized *E. coli* cells harbouring *Bm*GDH (*E. coli* BL21(DE3)/GDH or *E. coli* D4/GDH, 20 g l^{-1}) and PBS (100 mM, pH 8.0) were incubated at 30°C and 200 rpm for 6 h. The extraction was conducted as described previously.

CRISPR-Cas9 mediated gene deletions in E. coli *BL21 (DE3)*

The genes adhP, adhE, yahK and nemA were deleted from *E. coli* BL21 (DE3) using a reported two-plasmid

CRISPR-Cas9 gene-editing system. The guide sequence was designed by CRISPOR tool (http://crispor.tefor.net/crispor.py).

Sequences of the primers used for the gene deletion in this study were listed in the supplemental material (Table S5). The vector pTarget was employed to construct plasmid encoding guide RNA for Cas9 endonuclease. With the *E. coli* BL21(DE3) genomic DNA as template, the upstream and downstream homologous arms of target genes were amplified and fused by overlap PCR. Then, the fusion gene fragment and respective pTarget were co-transformed into electrocompetent *E. coli* BL21(DE3) carrying pCas vector. The gene deletion of *E. coli* BL21 (DE3) was confirmed by sequencing PCR products of colony PCR. Plasmids pCas and pTarget were then cured by referring to prior research (Liu *et al*., 2021a,2021b).

Construction and preparation of biocatalyst

The glucose dehydrogenase (GDH) gene *gdh* from *B. megaterium* was constructed in vector pET-28a(+) (pET28a-*gdh*). Subsequently, the open reading frame of the *gdh* gene's region in pET28a-*gdh* was amplified by PCR. Then, the open reading frame was inserted into the *Hind* III site of vector pACYC184. As a result, the expression plasmids were designated pACYC184-*gdh*. In order to construct recombinant cells for co-expression, the pACYC184-*gdh* and pET21d-*oye2p* (or pET21d-Y84V) were transformed into *E. coli* BL21(DE3) and *E. coli* D4 respectively. The recombinant cells were cultivated at the same conditions as described above. Then, the collected recombinant cells were washed twice with 0.9% NaCl solution and lyophilized in a freeze-dryer at −40°C for 12 h.

Optimization of the reaction conditions

The conditions were optimized using 0.5 ml of a reaction mixture in a 2 ml Eppendorf tube. The standard bioreductions contained 200 mM of (*E*/*Z*)-citral, 250 mM of glucose, 100 mM PBS (pH 8.0), 0.2 mM of NAD^+ and 50 g l^{-1} of lyophilized cells (D4-VG) and were carried out at 30°C, 200 rpm for 2 h. All variables were optimized one by one, and previously optimized conditions always remained the same.

For optimization of temperature, the reactions were carried out at pH 8.0 and 200 rpm with temperatures ranging between 20°C and 37°C. To optimize the pH value, the reaction was run at 30°C, 200 rpm and a pH range of 6.0–10.0 using sodium phosphate buffer (pH 6.0–8.5) and glycine/NaOH buffer (pH 8.5–10). To test the effect of NAD^+ concentration on bioreductions, the conditions were pH 8.0, 30°C, 200 rpm and an NAD^+ concentration between 0 and 0.5 mM. The reactions were stopped by the addition of ethyl acetate, and the organic phase was used for GC analysis.

*Preparative synthesis of (*R*)-citronellal*

To validate the industrial scale application, 20 ml-scale bioreduction for citral was accomplished in a round-bottomed flask. The reaction mixture contained 100 mM PBS (pH 8.0), 75 g l^{-1} lyophilized cells (D4-VG or D4-YG), 106.6 g l^{-1} (*E*/*Z*)-citral, 138.6 g l^{-1} glucose and 0.1 mM NAD^+. The pH value was adjusted to 8.0 by titrating 2.0 M Na_2CO_3, and the mixtures were incubated at 30°C with shaking at 200 rpm.

Samples were withdrawn at regular intervals and extracted twice with an equal volume of ethyl acetate. The organic phase was separated and collected by centrifugation at 12 000 rpm for 10 min. To determine the conversion and yield of the reaction, the combined organic phase was dehydrated using anhydrous Na_2SO_4 and used for gas chromatography (GC).

The space-time yield of citronellal was calculated according to the following equation:

$$\text{Space - time yield of citronellal } \left(\text{g l}^{-1}\,\text{day}^{-1}\right) = \frac{[S]_{\text{citronellal}}}{\text{Time}}, \quad (3)$$

where $[S]_{\text{citronellal}}$ is the concentration of citronellal at the end of reaction, Time was the reaction time at the end.

All reactions and assays were carried out in triplicate.

Analytical procedures

The conversion and yield were analysed by GC (7820A; Agilent, Santa Clara, CA, USA). The conversion and yield were determined using an HP-5 column (30 m × 0.32 mm × 0.25 μm; Agilent). The GC conditions were the injection and flame ionization detector temperatures were 220 and 250°C respectively; nitrogen was used as the carrier gas (1 ml min^{-1}) with a split ratio of 10:1; the initial column temperature was 90°C for 2 min followed by a 10°C min^{-1} increase to 150°C for 4 min. The retention times of citronellal, citronellol, nerol, neral, geraniol and geranial were 4.20, 5.48, 5.55, 5.79, 6.17 and 6.43 min respectively. The stereoselective assay of citronellal was performed by a GC system equipped with a β-DEX 225 column (30 m × 0.25 mm × 0.25 μm; Supelco, Bellafonte, PA, USA). The temperature program involved 90°C for 35 min followed by a 5°C min^{-1} increase to 160°C for 2 min; then, it was heated to 200°C at 10°C min^{-1} and held for 2 min. The retention times of (*S*)- and (*R*)-citronellal were 40.64 and 40.81 min respectively.

Acknowledgements

This work was supported by the National Key Research and Development Program of China (No. 2021YFC2102100), the Natural Science Foundation of Shanghai (No. 19ZR1412700), the Fundamental Research Funds for the Central Universities (No. 22221818014) and partially supported by the Open Funding Project of the State Key Laboratory of Bioreactor Engineering.

Conflicts of interest

The authors declare no conflict of interest.

References

Amato, E.D., and Stewart, J.D. (2015) Applications of protein engineering to members of the old yellow enzyme family. *Biotechnol Adv* **33:** 624–631.

Baik, S.H., Ide, T., Yoshida, H., Kagami, O., and Harayama, S. (2003) Significantly enhanced stability of glucose dehydrogenase by directed evolution. *Appl Microbiol Biotechnol* **61:** 329–335.

Bougioukou, D.J., Walton, A.Z., and Stewart, J.D. (2010) Towards preparative-scale, biocatalytic alkene reductions. *Chem Commun* **46:** 8558–8560.

Carbonell, P., Wong, J., Swainston, N., Takano, E., Turner, N.J., Scrutton, N.S., *et al*. (2018) Selenzyme: enzyme selection tool for pathway design. *Bioinformatics* **34:** 2153–2154.

Etzold, B., Jess, A., and Nobis, M. (2009) Epimerisation of menthol stereoisomers: kinetic studies of the heterogeneously catalysed menthol production. *Catal Today* **140:** 30–36.

Hepworth, L.J., France, S.P., Hussain, S., Both, P., Turner, N.J., and Flitsch, S.L. (2017) Enzyme cascades in whole cells for the synthesis of chiral cyclic amines. *ACS Catalysis* **7:** 2920–2925.

Hooft, R.W.W., Sander, C., and Vriend, G. (1997) Objectively judging the quality of a protein structure from a Ramachandran plot. *Comput Appl Biosci* **13:** 425–430.

Kress, N., Rapp, J., and Hauer, B. (2017) Enantioselective reduction of citral isomers in NCR ene reductase: analysis of an active-site mutant library. *Chembiochem* **18:** 717–720.

Kunjapur, A.M., Tarasova, Y., and Prather, K.L. (2014) Synthesis and accumulation of aromatic aldehydes in an engineered strain of *Escherichia coli*. *J Am Chem Soc* **136:** 11644–11654.

Lenardão, E.J., Botteselle, G.V., Azambuja, F.D., Perin, G., and Jacob, R.G. (2007) Citronellal as key compound in organic synthesis. *Tetrahedron* **63:** 6671–6712.

Liu, G., Li, S., Shi, Q., Li, H., Guo, J., Ouyang, J., *et al*. (2021a) Engineering of *Saccharomyces pastorianus* old yellow enzyme 1 for the synthesis of pharmacologically active (S)-profen derivatives. *Molecular Catalysis* **507:** 111568.

Liu, Y., Mao, X., Zhang, B., Lin, J., and Wei, D. (2021b) Modification of an engineered *Escherichia coli* by a combinatorial strategy to improve 3,4-dihydroxybutyric acid production. *Biotech Lett* **43:** 2035–2043.

Lüthy, R., Bowie, J.U., and Eisenberg, D. (1992) Assessment of protein models with three-dimensional profiles. *Nature* **356:** 83–85.

Maeda, H., Yamada, S., Itoh, H., and Hori, Y. (2012) A dual catalyst system provides the shortest pathway for L-menthol synthesis. *Chem Commun* **48:** 1772–1774.

Martí-Renom, M.A., Stuart, A.C., Fiser, A., Sánchez, R., Melo, F., and Šali, A. (2000) Comparative protein structure modeling of genes and genomes. *Annu Rev Biophys* **29:** 291–325.

Morris, G.M., Huey, R., Lindstrom, W., Sanner, M.F., Belew, R.K., Goodsell, D.S., and Olson, A.J. (2009) AutoDock4 and AutoDockTools4: automated docking with selective receptor flexibility. *J Comput Chem* **30:** 2785–2791.

Mueller, N.J., Stueckler, C., Hauer, B., Baudendistel, N., Housden, H., Bruce, N.C., and Faber, K. (2010) The substrate spectra of pentaerythritol tetranitrate reductase, morphinone reductase, N-ethylmaleimide reductase and estrogen-binding protein in the asymmetric bioreduction of activated alkenes. *Adv Synth Catal* **352:** 387–394.

Ni, Y., Yu, H.L., Lin, G.Q., and Xu, J.H. (2014) An ene reductase from *Clavispora lusitaniae* for asymmetric reduction of activated alkenes. *Enzyme Microb Technol* **56:** 40–45.

Salminen, E., Virtanen, P., and Mikkola, J.P. (2014) Alkaline ionic liquids applied in supported ionic liquid catalyst for selective hydrogenation of citral to citronellal. *Front Chem* **2:** 3.

Toogood, H.S., and Scrutton, N.S. (2019) Discovery, characterisation, engineering and applications of ene reductases for industrial biocatalysis. *ACS Catalysis* **8:** 3532–3549.

Yanto, Y., Yu, H.H., Hall, M., and Bommarius, A.S. (2010) Characterization of xenobiotic reductase A (XenA): study of active site residues, substrate spectrum and stability. *Chem Commun* **46:** 8809–8811.

Ying, X., Yu, S., Huang, M., Wei, R., Meng, S., Cheng, F., *et al*. (2019) Engineering the enantioselectivity of yeast old yellow enzyme OYE2y in asymmetric reduction of (E/Z)-citral to (R)-Citronellal. *Molecules* **24:** 1057–1071.

Zheng, L., Lin, J., Zhang, B., Kuang, Y., and Wei, D. (2018) Identification of a yeast old yellow enzyme for highly enantioselective reduction of citral isomers to (R)-citronellal. *Bioresour Bioprocess* **5:** 9.

Zhou, J., Wang, C., Yoon, S.H., Jang, H.J., Choi, E.S., and Kim, S.W. (2014) Engineering Escherichia coli for selective geraniol production with minimized endogenous dehydrogenation. *J Biotechnol* **169:** 42–50.

Zuliani, A., Cova, C.M., Manno, R., Sebastian, V., Romero, A.A., and Luque, R. (2020) Continuous flow synthesis of menthol via tandem cyclisation–hydrogenation of citronellal catalysed by scrap catalytic converters. *Green Chem* **22:** 379–387.

Supporting information

Additional supporting information may be found online in the Supporting Information section at the end of the article.

Fig. S1. (A) The Verify-3D analysis of OYE2p model evaluation. (B) The Ramachandran plot of OYE2p model evaluation.

Fig. S2. Multiple sequence alignment of OYE2p with the other five OYEs including *Saccharomyces pastorianus* OYE1, *Scheffersomyces stipites* OYE2.6, *Saccharomyces cerevisiae* OYE3, *Kluyveromyces lactis* KYE1, *Meyerozyma guilliermondii Mg*ER. Substrate binding and catalytic residue are marked with a triangle.

Fig. S3. SDS-PAGE analysis of supernatant of OYE2p alanine mutants. The expected molecular weight (MW) of mutants were around 44 kDa. Lane M: Protein molecular weight marker; Lane1: WT; Lane2: T39A; Lane3: M41A; Lane 4: Y84A; Lane 5: W118A; Lane 6: H193A; Lane 7: N196A; Lane 8: R245A; Lane 9: F252A; Lane 10: N253A; Lane 11: P297A; Lane 12: F298A; Lane 13: Y377A.

Fig. S4. SDS-PAGE analysis of supernatant of OYE2p Y84 site-saturation mutants. The expected molecular weight (MW) of mutants were around 44 kDa. Lane M: Protein molecular weight marker.

Fig. S5. Docking and molecular dynamic simulation analysis of WT and Y84V. (A) Molecular docking of (*Z*)-citral into the active sites of WT. (B) Distance between hydroxyl group of Tyr198 and α-C of (*Z*)-citral in Y84V-(*Z*)-citral complex (red) and WT-(*Z*)-citral complex (black). (C) Distribution of the distance between hydroxyl group of Tyr198 and α-C of (*Z*)-citral in Y84V-(*Z*)-citral complex (red) and WT-(*Z*)-citral complex (black). (D) Molecular docking of (*Z*)-citral into the active sites of Y84V. (E) Distance between N5 atom of FMN and β-C of (*Z*)-citral in Y84V-(*Z*)-citral complex (red) and WT-(*Z*)-citral complex (black). (F) Distribution of the distance between N5 atom of FMN and β-C of (*Z*)-citral in Y84V-(*Z*)-citral complex (red) and WT-(*Z*)-citral complex (black).

Fig. S6. The volume of the substrate-binding pocket was calculated by pocasa 1.1. (A) WT, (B) Y84V.

Fig. S7. Tyr84 exist in the catalytic centre of ene reductases from OYE superfamily.

Fig. S8. SDS-PAGE analysis of the purified AdhP, AdhE and YahK. M: Molecular weight marker; 1: purified AdhP; 2: purified AdhE; 3: purified YahK.

Fig. S9. Colonies PCR validation of the *adhP*, *nemA*, *adhE* and *yahK* knockout. Marker: Trans 2K plus II marker; -: *E. coli* BL21(DE3); +: *E. coli* BL21(DE3) D4.

Fig. S10. SDS-PAGE analysis of the heterologous expression of Y84V and *Bm*GDH in *E. coli* BL21(DE3) and *E. coli* D4. M: Molecular weight marker; T: whole-cell lysate; S: supernatant; P: precipitate.

Fig. S11. GC analysis of citronellal and citronellol in reduction in (*E*/*Z*)-citral using BL21-VG and D4-VG.

Fig. S12. Synthesis of (*R*)-citronellal by *E. coli* D4/OYE2p/GDH (D4-YG). Reaction conditions: 100 mM PBS (pH 8.0), 75 g/L D4-YG (lyophilized cells), 106.6 g/L (*E*/*Z*)-citral, 138.6 g/L glucose, 0.1 mM NAD^+ and at 30°C.

Table S1. The primers for alanine scanning in OYE2p.

Table S2. The primers for site-saturation mutation of Y84 in OYE2p.

Table S3. Reaction equations in SMILES format.

Table S4. The primers for construction of expression plasmids.

Table S5. The primers for gene deletions in *E. coli* BL21 (DE3).

